Theor Chim Acta (1994) 88: 131–145

Theoretica Chimica Acta

Ab initio calculations of the rotationally resolved infrared spectrum of KNa_2^+

Feng Wang and Ellak I. von Nagy-Felsobuki
Department of Chemistry, The University of Newcastle, Callaghan, NSW 2308, Australia

Received February 1, 1993/Accepted August 19, 1993

Summary. Ab initio variational calculations were performed on the rotationally resolved infrared spectrum of KNa_2^+. A discrete potential energy surface was generated using the configuration interaction ansatz coupled with the frozen core approximation, from which an analytical representation was obtained using a power series expansion employing a Dunham expansion variable. This force field was embedded in an Eckart–Watson rovibrational Hamiltonian, from which eigenfunctions and eigenenergies were calculated. An SCF dipole moment surface was generated and used to calculate absolute line intensities and square dipole matrix elements between the vibrational ground state and the lowest-lying excited states for some of the most intense transitions within the P, Q and R branches.

Key words: KNa_2^+ – Rotationally resolved infrared spectrum – Potential energy surface

1 Introduction

Theoretical studies of alkali cluster ions have focussed on their electronic structure, stability and equilibrium geometry [1]. Interest in these cluster ions is due to the significant role they play in a number of technological processes [2] (which in part arises from the low ionisation potentials and electron affinities of the alkali metal atoms). Although most investigations have centred on the homogeneous cluster ions [3], work on the heterogeneous species has gathered momentum (due to their observations in supersonic expansions [4, 5]). Recently, pseudopotential [6, 7] and all electron methodologies [1, 8–11] have been utilised in studies of the electronic structure of clusters X_2Y^+(X, Y = Li, Na, K). Thus far, no experimental data is available on their rovibrational structure, although such information would be valuable with respect to their detection [2].

Over the last decade there has been a rapid increase in computer power. Nevertheless, attempts of solving the "complete" molecular Schrodinger equation are still not common place (even for electron-sparse molecules). Here "complete" is defined in terms of the construction of a Born–Oppenheimer potential energy (PE)

Correspondence to: E. I. von Nagy-Felsobuki

surface to variationally solving a rovibrational Hamiltonian [12]. Perhaps the most celebrated example in the literature is the unravelling of the rovibrational structure for the ground electronic state of H_3^+. Quantal investigations near the potential energy minimum of its infrared spectrum have predicted and substantiated experimental observations [13, 14]. Yet it still appears that quantal calculations resolving the spectra near the ion dissociation energy [15] of this simple two-electron system will not be forth coming in the immediate future.

For electron-dense molecules, more speculative configuration interaction (CI) surfaces need to be constructed. Basis set limitations and simple CI truncations have to be employed in order to make computations tractable. For example, in the case of H_2O^+ Weis et al. [16] employed a truncated multiconfigurational reference CI (MRCI) wavefunction in order to calculate a 50 point discrete PE surface (which Wang and von Nagy-Felsobuki [17] used in their subsequent rovibrational calculations). Further, PE surfaces have been constructed using even simpler CI truncations (such as from single and double substitutions from a single reference Hartree–Fock determinant; labelled SDCI). For molecules involving second and third row atoms even more drastic approximations are often employed; that is, the CI sub-space is usually truncated to the valence molecular orbitals (coined the "frozen-core" approximation; labelled FC). Alternatively for X_2Y^+ (X, Y = Li, Na, K) clusters, Pavolini and Spiegelmann [7] have resorted to a pseudopotential CI methodology in which core–core and core–valence interactions are replaced by simple functional forms, thereby alleviating the need to incorporate all the electrons in the calculations. All of these approaches have a common thread: to produce PE surfaces which are tractable, yet spectroscopically predictive.

In the case of triatomic molecules, the Eckart–Watson rovibrational Hamiltonians are problematic [8–12, 18], since Eckart's notion of an embedded equilibrium geometry necessarily precludes a smooth transition in the mass dependent operator (termed the Watson operator) for bent and linear nuclear configurations [19, 20]. This led Tennyson and Sutcliffe [21] to develop a rovibrational Hamiltonian in terms of a body-fixed scattering coordinate system. On the other hand, von Nagy-Felsobuki and coworkers [8] have developed the most general form of the Eckart–Watson Hamiltonian, which is applicable to bent triatomic systems not undergoing large amplitudes of vibration. The rovibrational Hamiltonian is based on rectilinear displacement coordinates for a molecule with C_S symmetry and so collapses to the D_{3h} and C_{2v} Hamiltonians developed by Carney et al. [22, 23].

Recently, it was demonstrated that for Li_3^+, the scattering coordinate Hamiltonian and solution algorithm of Tennyson and Sutcliffe [24] yielded essentially the same vibrational band origins near the potential energy minimum as the normal coordinate approach developed by von Nagy-Felsobuki and coworkers [25]. These vastly different solution algorithms (employing the same electronic force field [26, 27]) gave the same assignment and moreover, yielded the first ten vibrational band origins of $^7Li_3^+$ and $^6Li^7Li_2^+$ to within 0.03 cm^{-1} respectively. Thus, both approaches have properly converged in describing the small amplitudes of vibration for this molecule.

As an extension of our earlier work on the rovibrational structure of Li_3^+ [8, 9, 25–27], Li_2Na^+ [8, 9], $LiNa_2^+$ [8, 9], $KLiNa^+$ [8, 9], K_2Li^+ [10] and Na_3^+ [11], we wish to report a variational calculation of the rotational energy levels of the low-lying vibrational states for the ground electronic state of KNa_2^+. Although the PE surface reported here is speculative, the motivation for this investigation is to encourage and moreover, possibly assist experimentalist in detecting and identifying the rovibrational structure of KNa_2^+.

2 Computational details and results

Ab initio electronic calculations were performed using the GAUSSIAN 88 suite of programmes [28] within the SDCI/FC ansatz. Size-consistency cannot be properly accounted for using the Davidson's correction [29], since the frozen-core approximation reduces the correlation problem to a two-electron problem.

For sodium, Huzinaga and Klobukowski [30] (16*s*, 9*p*) primitive basis was used and supplemented with diffuse *d* and *f* polarisation functions (both with a partially optimised exponent of 0.16) yielding a (16*s*9*p*1*d*1*f*)/[10*s*6*p*1*d*1*f*] contracted basis. Similarly for potassium, a primitive basis (20*s*13*p*) [30] was employed, supplemented with *d* and *f* polarisation functions with partially optimised exponents of 0.16 and 0.09 respectively. This gives a (20*s*13*p*1*d*1*f*/15*s*8*p*1*d*1*f*) contracted basis set. Similar basis sets have been employed in generating the PE surfaces of Li_2Na^+ [8], $LiNa_2^+$ [8], $KLiNa^+$ [8], K_2Li^+ [10] and Na_3^+ [11].

To select electronic grid on the energy hypersurface the strategy employed was to choose points coincident with the quadrature points required by our numerical potential energy integrator (which in our case is the Harris, Engerholm and Gwinn or HEG quadrature scheme [31]), thereby reducing the errors associated with the analytical fit. A set of data points were initially calculated along the diagonal of each vibrational coordinates, within the prescribed integration limits of the numerical HEG scheme. To these points an analytical function was fitted, giving a preliminary surface from which 8000 HEG quadrature points could be selected. Electronic energies were calculated at a vastly reduced subset of points near the potential energy minimum, with additional points calculated in selected regions in order to ensure a "well behaved" analytical surface [8]. Table 1 details the full 66 point discrete PE surface of KNa_2^+.

In numerical rovibrational calculations it is important that the embedded force field accurately interpolates between calculated points on the energy hypersurface. In order to obtain an accurate analytical representation of the discrete ab initio surface, various power series expansions [32–36] and Padé approximant expansions [35–36] were examined. Of all the analytical representations investigated, the sixth-order power series expansion with the Dunham expansion variable was found to give the "best" [8] fit. In order to ensure that the analytical PE surface was free from singularities in the integration region, it was necessary to zero the singular values σ_{42}, σ_{44-48}. Table 2 lists the analytical representation of the PE surface of KNa_2^+, which was used in the subsequent vibrational and rovibrational calculations. Figure 1 gives the corresponding contour plots of the PE surface in terms of rectilinear vibrational coordinates (labelled at *t* coordinates).

The vibrational Hamiltonian used in this investigation is the *t* coordinate Hamiltonian derived by Carney et al. [23]. The Hamiltonian has the form

$$H = -\frac{\hbar^2}{2M_r}\sum_{i=1}^{3}\frac{\partial^2}{\partial t_i^2} - \frac{\hbar^2}{2I'_{zz}(t_1)}\left(t_3\frac{\partial}{\partial t_2} - t_2\frac{\partial}{\partial t_3}\right)^2 - \frac{\hbar^2}{8}\sum_{\alpha}\mu_{\alpha\alpha} + \hat{V}, \qquad (1)$$

where the first term is the vibrational kinetic energy operator, the second term is the vibrational angular momentum operator and the third term is the Watson operator, which is a mass dependent contribution to the potential energy operator (the latter given by the last term).

The Watson operator is the sum of the diagonal elements of the reciprocal effective moment of the inertial tensor and a perturbation expression for this operator was derived by von Nagy-Felsobuki and coworkers [10] in terms of the

Table 1. Discrete potential energy surface of the ground electronic state of KNa_2^+

R_{Na-K}/a.u.	$R_{Na'-K}$/a.u.	$R_{Na-Na'}$/a.u.	E/E_h
7.8284	7.8284	6.3098	−922.7840
8.0151	8.0151	6.4615	−922.7838
7.6417	7.6417	6.1605	−922.7837
8.2951	8.2951	6.6872	−922.7828
7.3617	7.3617	5.9347	−922.7824
8.7618	8.7618	7.0635	−922.7798
6.8950	6.8950	5.5585	−922.7768
9.2285	9.2285	7.4397	−922.7756
6.4283	6.4283	5.1823	−922.7654
9.6952	9.6952	7.8159	−922.7707
5.9616	5.9616	4.8060	−922.7459
10.6286	10.6286	8.5684	−922.7601
5.0282	5.0282	4.0536	−922.6706
7.7752	7.7753	6.5430	−922.7838
7.8845	7.8845	6.0789	−922.7837
7.7009	7.7012	6.8911	−922.7828
7.9738	7.9741	5.7309	−922.7823
7.5921	7.5934	7.4712	−922.7801
8.1361	8.1373	5.1508	−922.7760
7.5029	7.5057	8.0512	−922.7767
8.3143	8.3168	4.5707	−922.7625
7.4340	7.4391	8.6313	−922.7732
8.5075	8.5118	3.9907	−922.7384
7.3592	7.3706	9.7915	−922.7672
7.6790	7.9807	6.3162	−922.7839
8.2036	7.4495	6.3351	−922.7834
7.0857	8.5932	6.4216	−922.7818
8.9598	6.7004	6.5393	−922.7788
6.3559	9.3652	6.7334	−922.7744
10.1058	5.6075	7.1940	−922.7593
7.9619	6.6935	6.2669	−922.7805
8.0711	8.0712	6.2294	−922.7838
7.5886	7.5886	6.3925	−922.7837
7.6978	7.6979	5.9285	−922.7833
8.5215	8.5226	8.2236	−922.7748
9.0660	9.0670	5.9033	−922.7793
6.5815	6.5847	7.2988	−922.7721
7.3905	7.3934	3.8183	−922.7288
9.2703	9.2743	10.1363	−922.7614
10.3504	10.3540	5.4956	−922.7693
9.5659	9.5662	8.3960	−922.7681
8.1649	7.8632	6.4646	−922.7837
7.4923	7.7940	6.1659	−922.7836
9.5138	8.0061	7.1532	−922.7787
5.7875	8.0460	5.8317	−922.7684
11.2046	8.1927	8.1435	−922.7688
9.3222	10.4921	8.0484	−922.7681
11.9674	7.4592	8.5422	−922.7654
7.6248	7.9285	6.5481	−922.7837
8.0332	7.7338	6.0823	−922.7837
6.8237	8.3796	7.5649	−922.7769
9.2299	7.0587	5.4282	−922.7756
5.8633	9.0422	8.9448	−922.7575
7.0404	7.8394	8.6526	−922.7722

Table 1. (Continued)

R_{Na-K}/a.u.	$R_{Na'-K}$/a.u.	$R_{Na-Na'}$/a.u.	E/E_h
10.6404	6.5277	5.2774	−922.7652
7.7881	8.5543	7.2927	−922.7805
8.0739	8.8153	6.1373	−922.7824
7.8759	7.1369	5.3832	−922.7782
6.8552	7.6228	6.5429	−922.7813
7.7114	10.8679	10.4060	−922.7589
9.7008	13.8070	6.1853	−922.7671
7.6978	12.4814	12.5518	−922.7514
9.2169	6.8902	8.0318	−922.7731
4.5789	6.9285	6.2206	−922.7303
9.2021	8.4165	9.7754	−922.7653
7.8549	10.7089	5.8191	−922.7759

Table 2. Fitting coefficients of the sixth-order Dunham potential energy surface of KNa_2^+ [a]

Expansion variable[b]	Coefficient	Expansion variable[b]	Coefficient
1	−922.784	$\rho_1^4\rho_3+\rho_2^4\rho_3$	−0.007
$\rho_1+\rho_2$	0.000	$\rho_1\rho_3^4+\rho_2\rho_3^4$	0.042
ρ_3	0.000	$\rho_1^3\rho_2^2+\rho_1^2\rho_2^3$	−0.265
$\rho_1^2+\rho_2^2$	0.116	$\rho_1^3\rho_3^2+\rho_2^3\rho_3^2$	−0.121
ρ_3^2	0.157	$\rho_1^2\rho_3^3+\rho_2^2\rho_3^3$	−0.189
$\rho_1\rho_2$	0.001	$\rho_1^3\rho_2\rho_3+\rho_1\rho_2^3\rho_3$	−0.262
$\rho_2\rho_3+\rho_1\rho_3$	−0.002	$\rho_1\rho_2\rho_3^3$	0.027
$\rho_1^3+\rho_2^3$	−0.282	$\rho_1^2\rho_2^2\rho_3$	0.046
ρ_3^3	−0.323	$\rho_1^2\rho_2\rho_3^2+\rho_1\rho_2^2\rho_3^2$	0.545
$\rho_1^2\rho_2+\rho_2^2\rho_1$	−0.016	$\rho_1^6+\rho_2^6$	−0.137
$\rho_1^2\rho_3+\rho_2^2\rho_3$	−0.018	ρ_3^6	−0.010
$\rho_1\rho_3^2+\rho_2\rho_3^2$	−0.011	$\rho_1^5\rho_2+\rho_2^5\rho_1$	0.068
$\rho_1\rho_2\rho_3$	0.116	$\rho_1^5\rho_3+\rho_2^5\rho_3$	0.052
$\rho_1^4+\rho_2^4$	0.321	$\rho_1\rho_3^5+\rho_2\rho_3^5$	−0.139
ρ_3^4	0.344	$\rho_1^4\rho_2^2+\rho_2^4\rho_1^2$	−0.120
$\rho_1^3\rho_2+\rho_2^3\rho_1$	0.077	$\rho_1^4\rho_3^2+\rho_2^4\rho_3^2$	−0.241
$\rho_1^3\rho_3+\rho_2^3\rho_3$	0.032	$\rho_1^2\rho_3^4+\rho_2^2\rho_3^4$	0.331
$\rho_1\rho_3^3+\rho_2\rho_3^3$	0.043	$\rho_1^4\rho_2\rho_3+\rho_2^4\rho_1\rho_3$	−0.006
$\rho_1^2\rho_2^2$	0.237	$\rho_1\rho_2\rho_3^4$	0.010
$\rho_1^2\rho_3^2+\rho_2^2\rho_3^2$	0.011	$\rho_1^3\rho_2^3$	−0.189
$\rho_1^2\rho_2\rho_3+\rho_1\rho_2^2\rho_3$	−0.023	$\rho_1^3\rho_3^3+\rho_2^3\rho_3^3$	0.304
$\rho_1\rho_2\rho_3^2$	−0.324	$\rho_1^3\rho_2^2\rho_3+\rho_1^2\rho_2^3\rho_3$	−0.087
$\rho_1^5+\rho_2^5$	−0.023	$\rho_1^3\rho_2\rho_3^2+\rho_1\rho_2^3\rho_3^2$	0.151
ρ_3^5	−0.176	$\rho_1^2\rho_2\rho_3^3+\rho_1\rho_2^2\rho_3^3$	0.043
$\rho_1^4\rho_2+\rho_2^4\rho_1$	−0.124	$\rho_1^2\rho_2^2\rho_3^2$	−0.148
$(\chi^2)^{1/2}$			-7.374×10^{-5}

[a] SVD analysis is used [23, 32] with singular values σ_{42}, σ_{44-48} being set to zero

[b] Dunham expansion variable has form: $(R_i-R_e)/R_e$ where R_i and R_e are the instantaneous and equilibrium bond distances respectively

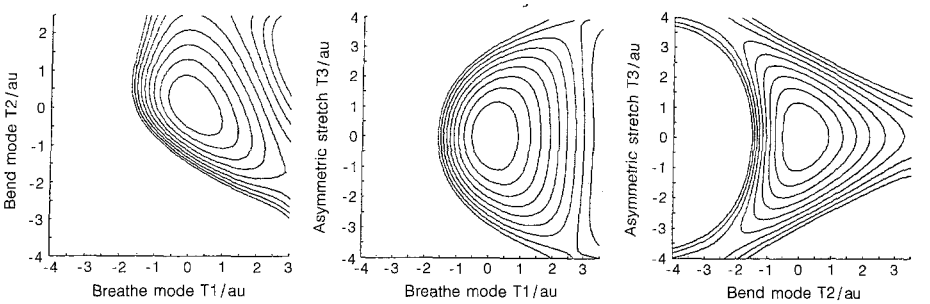

Fig. 1. Two-dimensional constant potential energy plots for the 6th order power series expansion using a Dunham expansion variable. The singular values σ_{42}, σ_{44}–σ_{48} are zeroed

t coordinates. A third-order Taylor series expansion for this operator is incorporated in the vibrational Hamiltonian, thereby circumventing difficulties which arise from the embedded singularities [8–12, 18].

The algorithm for our variational solution can be described as follows. The three one-dimensional eigenfunctions were obtained from a finite-element solution of a one-dimensional Hamiltonian expressed in terms of a single t coordinate. The first-order expansion of the Watson operator is diagonal in t coordinates and so was employed in the one-dimensional Hamiltonians. For each t coordinate, 1000 finite-elements were constructed within the following domains: t_1[−3.0, 4.2], t_2 [−2.2, 4.8], t_3 [−4.0, 4.0]. A three-dimensional configuration basis was then constructed from the three one-dimensional eigenfunctions [37]. The three-dimensional basis set was determined from all configurational products containing less than or equal to 13 nodes. Hence a total of 560 basis functions were employed in the three-dimensional solution. In the case of the three-dimensional Hamiltonian, the third-order expansion of the Watson operator was employed. The potential energy integrals were numerically evaluated using the HEG scheme [31], whereas all other integrals were evaluated using a sixteen point Gauss quadrature scheme. Finally, the secular determinant was constructed using Eq. (1) and diagonalised to yield vibrational eigenfunctions and eigenenergies, both of which are required for the rovibrational problem. Table 3 assigns the 20 lowest-lying vibrational band origins of KNa_2^+ using the solution algorithm.

The rovibrational Hamiltonian, spanned by the vibration basis set, is given by [23]

$$\hat{H}_{ij}^{\mathrm{VR}} = E_i\langle S\rangle_{ij} + 0.5\langle A\rangle_{ij}\hat{\Pi}_x^2 + 0.5\langle B\rangle_{ij}\hat{\Pi}_y^2 + 0.5\langle C\rangle_{ij}\hat{\Pi}_z^2 + 0.5\langle D\rangle_{ij}(\hat{\Pi}_x\hat{\Pi}_y + \hat{\Pi}_y\hat{\Pi}_x) + i/\hbar\langle F\rangle_{ij}\hat{\Pi}_z, \quad (2)$$

where E_i is the ith "pure" vibrational eigenenergy, $\langle S\rangle_{ij}$ is the vibrational overlap integral and $\hat{\Pi}$'s are the rotational angular-momentum operators, whose components refer to the molecule-fixed coordinate system. The A–D vibrational matrices are symmetric. The $\langle D\rangle$ and $\langle A\rangle$–$\langle B\rangle$ matrix elements couple adjacent odd or even values of K. The F matrix represents the Coriolis coupling that splits levels with non-zero K values (i.e. z axis angular momentum component) in this presence of vibrational angular momentum. Table 4 gives rotational matrix elements involving the lowest five vibrational eigenfunctions with the 0.5 factor in Eq. (2) being incorporated in the rotational constants and so they are labelled as A'–D'.

Table 3. Vibrational band origins of KNa_2^+ (/cm^{-1})

$\nu_1\nu_2\nu_3$	Symmetry	% weight[a]	Vibrational band origin[b]
000	A_1	98.2	0.00
001	B_1	96.7	70.91
100, 010	A_1	47.9, 45.8	85.57
010, 100	A_1	50.2, 47.3	136.95
002	A_1	93.7	141.52
101, 011	B_1	45.1, 42.5	155.53
110, 200, 020	A_1	41.9, 22.8, 19.9	170.85
011, 101	B_1	49.6, 46.6	207.64
003	B_1	88.9	211.87
020, 200	A_1	48.3, 45.2	222.05
102, 012	A_1	40.3, 37.4	225.18
111, 201, 021	B_1	36.4, 20.1, 16.9	239.90
210, 120, 300	A_1	27.5, 25.0, 10.5	255.86
110, 020, 200	A_1	47.0, 25.5, 23.5	272.85
012, 102	A_1	47.3, 45.6	278.03
004	A_1	82.5	281.95
021, 201	B_1	45.5, 42.7	291.82
103, 013	B_1	33.9, 30.7	294.55
030, 300, 120	A_1	32.8, 31.2, 12.9	306.87
112, 202, 022	A_1	28.7, 15.9, 13.1	308.67

[a] % Weight $= \{C_{ij}^2/\sum C_{ij}^2\}^{1/2} \times 100$

[b] The zero-point energy of KNa_2^+ is 147.85 cm^{-1}

Table 4. Rotational and Coriolis matrix elements of KNa_2^+ (/cm^{-1})[a]

Matrix element	A′	B′	C′	D′	F[b]
1 1	0.1314	0.0555	0.0389	−0.9648−11	0.1519−19
2 1	0.0000	0.0000	0.0000	−0.3991−02	0.1483−03
2 2	0.1321	0.0553	0.0387	0.1269−11	0.5334−19
3 1	0.0021	−0.0027	−0.0012	0.4237−12	0.6954−10
3 2	0.0000	0.0000	0.0000	−0.5816−03	0.5405−01
3 3	0.1313	0.0553	0.0388	0.6334−11	0.1175−18
4 1	0.0079	0.0004	0.0009	−0.6971−12	0.7836−10
4 2	0.0000	0.0000	0.0000	−0.2790−03	0.5766−01
4 3	−0.0003	0.0003	0.0001	0.3095−11	−0.1875−10
4 4	0.1306	0.0555	0.0388	−0.5256−11	−0.7897−19
5 1	0.0001	0.0003	0.0001	0.2066−11	−0.4834−10
5 2	0.0000	0.0000	0.0000	−0.5643−02	−0.9185−02
5 3	0.0002	−0.0001	0.0000	0.3206−10	−0.7302−10
5 4	0.0001	0.0000	0.0000	0.3208−11	0.3717−11
5 5	0.1328	0.0551	0.0386	0.1246−09	−0.3243−18

[a] The entry −0.3243−18 represents -0.3243×10^{-18}

[b] The F matrix elements have the relationship $F(i,j) = -F(j,i)$

Table 5. Rotational energy levels of KNa_2^+ for low-lying vibrational states (/cm^{-1})

E_v			0.000	70.906	85.573	136.947	141.525
J	K_a	K_c					
1	0	1	0.094	0.094	0.094	0.094	0.094
1	1	1	0.170	0.171	0.170	0.169	0.172
1	1	0	0.187	0.187	0.187	0.186	0.188
2	0	2	0.281	0.281	0.279	0.281	0.280
2	1	2	0.343	0.343	0.341	0.341	0.344
2	1	1	0.392	0.392	0.391	0.392	0.392
2	2	1	0.620	0.623	0.619	0.617	0.626
2	2	0	0.622	0.625	0.622	0.619	0.628
3	0	3	0.555	0.554	0.551	0.554	0.554
3	1	3	0.599	0.601	0.596	0.598	0.601
3	1	2	0.699	0.698	0.697	0.698	0.697
3	2	2	0.903	0.906	0.901	0.900	0.908
3	2	1	0.915	0.917	0.913	0.912	0.919
3	3	1	1.326	1.332	1.324	1.319	1.338
3	3	0	1.326	1.332	1.324	1.319	1.338
4	0	4	0.910	0.911	0.905	0.909	0.912
4	1	4	0.940	0.941	0.934	0.937	0.942
4	1	3	1.104	1.102	1.100	1.103	1.101
4	2	3	1.279	1.281	1.275	1.275	1.283
4	2	2	1.312	1.313	1.309	1.310	1.314
4	3	2	1.707	1.713	1.704	1.701	1.719
4	3	1	1.709	1.715	1.706	1.702	1.720
4	4	1	2.293	2.304	2.291	2.281	2.316
4	4	0	2.293	2.304	2.291	2.281	2.316
5	0	5	1.344	1.345	1.336	1.342	1.346
5	1	5	1.361	1.363	1.353	1.358	1.365
5	1	4	1.604	1.602	1.598	1.603	1.600
5	2	4	1.745	1.747	1.739	1.741	1.749
5	2	3	1.817	1.816	1.811	1.815	1.816
5	3	3	2.186	2.191	2.180	2.179	2.196
5	3	2	2.192	2.196	2.187	2.185	2.201
5	4	2	2.770	2.781	2.766	2.758	2.792
5	4	1	2.770	2.781	2.766	2.758	2.792
5	5	1	3.523	3.541	3.520	3.504	3.559
5	5	0	3.523	3.541	3.520	3.504	3.559

The rotational basis used was the plus and minus combinations of the regular symmetric top eigenfunction as detailed by Carney et al. [23]. The advantage of $R^{\pm}_{jkm}$ basis is that the corresponding matrix elements spanning the angular momentum operators are real. Rovibrational eigenfunctions and eigenenergies were obtained by diagonalisation H^{VR}. Table 5 gives the variationally calculated rotational eigenenergies up to J equals 5 for the low-lying vibrational states. To ensure convergence of the calculated eigenenergies, further calculations were employed using ten vibrational eigenfunctions and to the same J level. It was found that using five and ten vibrational eigenfunctions the mean difference for all the rotational level is 0.001 cm^{-1}.

Table 6. Spectroscopic constants of KNa_2^+ for the lowest five vibrational states (MHz)

κ	−0.6411	−0.6445	−0.6432	−0.6362	−0.6497
A+C	−0.5105+04	0.5126+04	0.5098+04	0.5080+04	0.5147+04
A−C	0.2773+04	0.2795+04	0.2778+04	0.2753+04	0.2816+04
τ_{AAAA}	−0.0429	0.1191	−0.2563	−0.0104	0.2785
τ_{BBBB}	−0.0705	−1.1764	0.8858	0.1847	−1.6919
τ_{CCCC}	0.1126	0.8181	−0.7161	−0.1644	1.2460
τ_{AACC}	0.7377	6.4148	−5.3407	−1.1815	9.7972
τ_{BBCC}	0.0976	0.5462	−0.5073	−0.1229	0.8522
τ_{AABB}	−0.8290	−6.8499	5.8783	1.3705	−10.4893
Reduction distortion constants					
Δ_J	0.0142	0.1322	−0.0787	−0.0218	0.1767
Δ_{JK}	−0.0441	−0.4243	0.2285	0.0489	−0.5700
Δ_K	0.0018	0.0876	0.0292	0.0140	0.0819
δ_J	−0.0017	−0.0810	0.0714	0.0122	−0.1231
δ_K	−0.2668	−0.5737	−1.4227	−0.5330	−0.7199
First-order centrifugal distortion constants					
D_J	0.0625	0.5272	−0.4264	−0.1020	0.7881
D_{JK}	−0.3338	−2.7947	2.3148	0.5301	−4.2385
D_K	0.2431	2.0630	−1.7094	−0.3870	3.1390
δ_J	−0.0017	−0.0810	0.0714	0.0122	−0.1231
R_5	0.2028	0.8527	0.2126	0.1506	1.2310
R_6	0.0241	0.1975	−0.1739	−0.0401	0.3057

Table 7. Expansion coefficients for dipole moment surface of KNa_2^+ [a]

Expansion variable	μ_X	Expansion variable	μ_Y
1	−0.88809	t_3	0.89173
t_1+t_2	0.49456	$t_3(t_1+t_2)$	−0.07601
$(t_1+t_2)^2$	0.12916	t_3^3	−1.68282
t_3^2	1.42193	$t_3(t_1+t_2)^2$	−0.51101
$(t_1+t_2)^3$	−0.34344	$t_3^3(t_1+t_2)$	1.14828
$t_3^2(t_1+t_2)$	1.83491	$t_3(t_1+t_2)^3$	1.41193
$(t_1+t_2)^4$	−0.10140	t_3^5	2.29763
t_3^4	−1.98692	$t_3(t_1+t_2)^4$	−0.61511
$t_3^2(t_1+t_2)^2$	−2.86799	$t_3^3(t_1+t_2)^2$	2.40774
$(t_1+t_2)^5$	0.11370		
$t_3^4(t_1+t_2)$	−8.14873		
$t_3^2(t_1+t_2)^3$	3.43453		

[a] All entries in atomic units

Table 6 gives the spectroscopic constants for KNa_2^+ obtained using a least-squares fit to the rovibrational eigenenergies. The definition of the reduced Hamiltonians has been given by Watson [38]. The fundamental frequencies and anharmonic constants could not be obtained within reasonable precision using a simple least-squares fitting procedure, since configuration eigenfunctions are

Table 8. Vibrational transition frequencies, square dipole matrix elements, Einstein coefficients[a], band strengths[a] and radiative lifetimes for KNa_2^+ [a]

j	i	ν_{ji} /cm^{-1}	μ_{ji}^2 /D^2	A_{ji}[b] /s^{-1}	B_{ji}[b] /10^{16} cm^3 erg^{-1} s^{-2}	S_{ji}[b] /atm^{-1} cm^{-2}	τ[c] /s
1	0	70.91	0.13+00	0.0141	23.7236	3.565	8.78
2	0	85.57	0.17+03	0.0000	0.0317	0.007	12.80
3	0	136.95	0.58−01	0.0467	10.9286	5.298	6.51
4	0	141.52	0.13−01	0.0118	2.4954	1.279	9.30
5	0	155.53	0.35−03	0.0004	0.0663	0.040	10.30
6	0	170.85	0.30−03	0.0005	0.0566	0.040	14.47
7	0	207.64	0.29−03	0.0008	0.0553	0.053	11.53
8	0	211.87	0.82−03	0.0024	0.1539	0.153	10.44
9	0	222.05	0.35−04	0.0001	0.0066	0.007	16.58

[a] Calculated at 300 K
[b] See ref. [27, 43, 49] for the formulae associated with the quantities
[b] Lifetime of the upper state. See ref. [27, 49] for the formula

Table 9. Rovibrational absorption line intensities (at 300 K) for ground states of KNa_2^+

v'	J'	K_a'	K_c'	v''	J''	K_a''	K_c''	Branch P, Q, R	ν_{AX}[a]	S_{AX}[b]	R_{AX}^2[c]
0	3	3	0	0	4	0	4	−1	0.42	0.139−06	0.264+01
0	4	2	2	0	4	0	4	0	0.40	0.192−06	0.391+01
0	4	3	2	0	3	3	1	1	0.38	0.189−06	0.426+01
1	1	1	0	0	2	2	1	−1	70.47	0.159−03	0.124+00
1	3	1	2	0	3	1	2	0	70.91	0.161−03	0.124+00
1	4	1	3	0	3	1	3	1	71.41	0.177−05	0.135−02
2	3	3	1	0	4	4	1	−1	84.60	0.299−06	0.168−03
2	2	1	2	0	2	2	1	0	85.29	0.305−06	0.167−03
2	4	2	3	0	3	1	2	1	86.15	0.301−06	0.168−03
3	2	1	1	0	3	1	3	−1	136.74	0.253−05	0.605−03
3	3	3	1	0	3	2	1	0	137.35	0.233−03	0.554−01
3	3	2	2	0	2	2	0	1	137.22	0.236−03	0.560−01
4	2	2	0	0	3	1	3	−1	141.55	0.631−06	0.142−03
4	3	3	1	0	3	1	2	0	142.16	0.590−04	0.132−01
4	3	3	0	0	2	2	1	1	142.24	0.587−04	0.131−01

[a] Difference of eigenenergies between rovibrational states labelled as A and X, where A and X represent the upper and lower rovibrational states. All entries in unit of cm^{-1}
[b] Band strengths between rovibrational states labelled as A and X, where A and X represent the upper and lower rovibrational states. All entries in unit of atm^{-1} cm^{-2}. See ref. [16] for formula used
[c] Square of the dipole matrix element spanned by the rovibrational states are labelled as AX, where A and X represent the upper and lower rovibrational states. All entries in unit of D^2

sufficiently "mixed" to preclude a simple assignment to a single component of the configurational basis. However, following the usual prescription [39, 40] some of the spectroscopic constants were obtained from least-squares fits of rotational energy levels using the first five vibrational states.

Difficulties were encountered using the GAUSSIAN 88 package in the generation of the CI dipole moment surface [41]. Hence ab initio calculations of the discrete dipole moment surface of the ground electronic state of KNa_2^+ were performed at the Hartree–Fock SCF level. A 51 point dipole moment surface was calculated in terms of the t coordinates [10]. The grid used for the dipole moment surface differed from that used for the electronic energy calculations only with respect to its size. Points well away from the minimum energy geometry (i.e. displacements larger than 1.5 a.u.) were excluded in order to facilitate a more precise fit to an analytical representation. The geometry at each data point was rotated and/or reflected in order to coincide with the Eckart framework. The molecule was situated in the xy plane, with the origin coinciding with the centre of mass and the positive x axis bisecting the included angle for the C_{2v} symmetry. Table 7 gives the calculated regression coefficients for KNa_2^+ using the t coordinate expansion [10]. The coefficients clearly show that the non-linear regions are significant, since the linear coefficient is not necessarily the largest coefficient. However, it should not be forgotten that the fit represents an optimal regression and so reflects its utility as an interpolating function.

The vibrational eigenenergies, eigenfunctions and dipole moment functions were used in order to calculate the dipole moment matrix elements, Einstein transition probabilities (A_{ji} and B_{ji}), band strengths (S_{ji}) and vibrational radiative lifetimes (τ). Table 8 lists these quantities together with the calculated transition frequencies. The dipole transition matrix elements are calculated using the variational eigenfunctions and the transition matrix elements individual line intensities were calculated using the usual formula [42, 43] spanned by the rovibrational basis set. Table 9 gives the variationally calculated rovibrational absorption line intensities of KNa_2^+ for a selected number of transitions.

3 Discussion

There are few investigations on the electronic structure of the ground state of KNa_2^+. Pavolini and Spiegelmann [7] have optimised its geometry using a small basis set within a pseudopotential CI framework. Pseudopotential models cannot rigourously account for core–core and core–valence correlation effects, since they seek to reduce the all-electron problem to a valency only problem [44–46]. On the other hand, our approach for electronic studies on electron-dense systems [8–12] is to use sizeable basis sets within the all-electron SDCI/FC ansatz. A single reference treatment is justified if the leading coefficients in the CI wavefunction are large and nearly constant at small displacements from the equilibrium geometry. In the case of the positive ions of the alkaline-earth oxides, fluorides and hydroxides Partridge et al. [47] have shown that SDCI wavefunction is capable of yielding accurate spectroscopic parameters when compared with experiment. Justification from employing the FC approximation is less satisfactory on theoretical grounds. However, comparison of the low-lying vibrational band origins of Li_3^+ using SDCI/Full with the SDCI/FC levels of theory [8] does give some credence for using the more tractable theory in the case of the electron-dense systems, provided that it is used in regions of small rectilinear displacements from the minimum.

At SDCI/FC level of theory the minimum energy structure of KNa_2^+ is of C_{2v} symmetry with an energy of $-992.7840 E_h$. The predicted equilibrium structural parameters (R_{KNa}, NaKNa bond angle) are ($7.83 a_0$, 47.55^0) which compares

well with the Hartree–Fock pseudopotential value of ($7.16a_0$, 46.51^0) [6] and pseudopotential CI value of ($7.58a_0$, 47.40^0) [7]. Absolute differences in the predicted structural parameters between the two CI levels theory are ($0.25a_0$, 0.15^0), which is in the range of differences between the pseudopotential CI method and other all-electron calculations. For example, in the case of Na_3 absolute differences of ($0.10a_0$, 11.5^0) occur [7].

The quadrature points used by the HEG numerical potential energy integrator were weighted to be coincident with the points of the discrete electronic energy surface in order to minimise the error of fit at these points of the energy hypersurface. Further, it should be stressed that the power series with the smallest $(\chi^2)^{1/2}$ is not necessarily the "best" fit to a PE surface [8, 35, 36], since numerical graphical inspections confirm that non-physical behaviour (e.g. singularities) can occur in the numerical integration region for fits with low $(\chi^2)^{1/2}$. It is therefore important that the analytical representation is consistent with anticipated physical properties [8, 35, 36]. Previously, for Li_2Na^+, $LiNa_2^+$, $KLiNa^+$ and Na_3^+, von Nagy-Felsobuki and coworkers [8, 10] have detailed Padé force fields of order $P(6,4)$, $P(4,5)$, $P(3,3)$ and $P(4,6)$ with $(\chi^2)^{1/2}$ of 2.5×10^{-7}, 3.8×10^{-7}, 4.4×10^{-5} and $3.5 \times 10^{-5} E_h$ respectively. However, for K_2Li^+ [11] the force field used was a power series expansion using the exponential Dunham variable which yielded a $(\chi^2)^{1/2}$ of $2.57 \times 10^{-4}\ E_h$. For KNa_2^+ Padé force fields for an array of different expansion variables and for different numerator and denominator orders could not eliminate singularities (even using SVD) in the integration region. Therefore, for KNa_2^+ a simple Dunham force field yielded the "best" result with $(\chi^2)^{1/2}$ of $7.4 \times 10^{-5}\ E_h$. As anticipated this more massive molecule resembles more nearly a spherical well for small rectilinear displacements from the PE minimum. Figure 1 demonstrates that the surface is smooth everywhere and with monotonically increasing repulsive walls within the integration region.

Vibrational band origins have been calculated for KNa_2^+ up to $\sim 310\ cm^{-1}$. The assignment is given in terms of the configurational basis in Table 3. The vibrational Hamiltonian used in this investigation has "full" mechanical anharmonicity as well as operators coupling the t vibrational modes. Hence, the assignment of the vibrational band origins is no longer simple since mixing can occur for configurational basis functions belonging to the same irreducible representation. That is, the configurational basis function (1 0 1) can readily mix with the (0 1 1), (0 0 3) etc. because each of these basis functions has B_1 symmetry. Therefore, the three-dimensional wavefunction for this delocalised model can no longer be expected to be diagonal in terms of the configurational basis functions. The percentage by weight of a basis function in the wavefunction given in Table 3 further emphasises this point. Using the percentage by weight as an assignment criterion the sequence of the five lowest-lying vibrational band origins are (0 0 1)<(1 0 0, 0 1 0)<(0 1 0, 1 0 0)<(0 0 2)<(1 0 1, 0 1 1), which is basically similar to the sequence given for $LiNa_2^+$ [8], although the second and third vibrational band origins have reversed their positions. For Li_2Na^+ [8] the same sequence has the (0 1 0) vibrational band origin lower in energy to the (2 0 0), whereas for K_2Li^+ [10] the vibrational eigenfunctions are far more "mixed". Nevertheless, it should be added that care needs to be taken against an over zealous interpretation due to the possibility of basis set incompleteness, even though our exploratory calculations showed convergence of the rotational levels to within $0.001\ cm^{-1}$. It is clear from the above discussion that the harmonic approximation within the framework of uncoupled modes (whilst intuitive) is far too simplistic for interpretation of the dynamics of this molecule.

Table 4 gives the rotational and Coriolis matrix elements spanned by the lowest five vibrational states. The centrifugal distortion are expected to be small near the potential energy minimum and the calculations reflect this anticipation by yielding values of less than 10^{-9} cm^{-1} for the diagonal elements. As would be anticipated, the off-diagonal elements of the Coriolis matrix elements are much larger than the diagonal elements, the latter of which are of order 10^{-18} cm^{-1}.

Table 5 highlights rotational energy levels for KNa_2^+ with respect to the lowest five vibrational states. The limiting case for the rotational levels of KNa_2^+ is Mulliken's prolate symmetric top. This is reflected by the Ray's asymmetry parameter, which is calculated to be -0.64 for the lowest-lying five vibrational states. Similarly, for Li_2Na^+ [8], $LiNa_2^+$ [8] and K_2Li^+ [10] Ray's asymmetry parameter is calculated to be -0.68, -0.82 and -0.99 respectively. Hence, the rotational energy levels (given in Table 5) are assigned within this framework of a prolate symmetric top and are calculated up to the J equals 5 level.

As high resolution rovibrational spectra are generally assigned by fitting rovibrational data to reduced Hamiltonians [38–40], Table 6 summarizes the calculated rotational spectroscopic constants obtained from our ab initio force fields and moreover, using our calculated rovibrational states. The calculations neglect spin-rotation interactions. Nevertheless, the signs and magnitude of these constants should be of use experimentalists in the spectroscopic rovibrational detection KNa_2^+.

As the dipole moment surface was calculated at the Hartree–Fock level the accuracy of the calculated transition probabilities, band strengths and vibrational radiative lifetimes must be treated with caution. However, Green [48] has concluded that at the Hartree–Fock limit the error associated with a dipole moment for a neutral diatomic molecule with a single sigma bond and using a double zeta basis set augmented with polarisation functions is of the order 0.1 to 0.2 D. The basis set used for KNa_2^+ certainly meets this criterion, although it is deficient with respect to producing a Hartree–Fock limit. Further, KNa_2^+ is bonded via single sigma bonds and so meets Green's [48] second criteria. Nevertheless, what is not known is the error variation of the dipole moment hypersurface over small amplitudes of displacements. There are too few discrete dipole moment surfaces reported in order to yield a estimate of the magnitude of error associated with a dipole hypersurface at the Hartree–Fock level, let alone at a CI level. Table 7 indicates that the linear expansion variables are not necessarily dominant and so care needs to be taken, since the error may not be uniform nor of the order of 0.2 D for small rectilinear displacements from the minimum energy. Moreover, it should also be noted that the accuracy of the slope of the dipole moment function is essential for calculation of the transition dipole matrix elements and so the presence of a non-uniform error would further degrade the spectroscopic quality of the surface.

Table 8 gives the calculated Einstein transition probabilities, band strengths and vibrational radiative lifetimes using vibrational eigenfunctions and eigenenergies. The transition probabilities and band strengths are given with respect to transitions from the ground vibrational state to the low-lying excited vibrational states. The life times given in Table 8 are for the upper states of the indicated transitions and so are the sums of the rates of spontaneous emission to all the lower-lying levels. For the C_{2v} point group there are no infrared forbidden transitions in the lowest-lying vibrational states, unlike Li_3^+ which has D_{3h} symmetry [49]. Hence the lifetimes of the excited vibrational states of KNa_2^+ are small for these transitions compared with those of Li_3^+ [49].

Contributions from the vibrational partition function were not neglected and were incorporated in the integrated adsorption band intensity which is given by [43, 49],

$$S_{ji} = \frac{\pi e^2}{Q_v} \frac{N_j f_{j \to i}}{mc^2 p} \frac{(1 - \exp(-hv_{ji}))}{kT}, \tag{3}$$

where the quantities in this equation have their usual meanings. Furthermore, the total partition function was used in order to determine the rotational line intensities, the formula of which is given Weis et al. [16]. Table 9 gives the absolute line intensities and the squares of the electric dipole transition matrix elements for some of the most intense transitions within the P, Q and R branches between the vibrational ground state and lowest-lying four excited vibrational states of KNa_2^+.

A portion of the rovibrational transitions should be experimentally accessible via laser spectroscopy, although no such data is currently available in the literature. Hence, it is hoped that these calculations will assist in the experimental spectroscopic detection of this molecule and moreover, will promote even more extensive theoretical calculations.

Acknowledgements. Calculations were performed using the VAX/VMS 3100 workstation and VAX/VMS 6620s, the latter made available by the generous support of the Computing Centre, University of Newcastle. We also wish to acknowledge the support of the Research Management Committee, The University of Newcastle and the Australian Research Council. Finally, we wish to acknowledge the Overseas Postgraduate Research Award and The University of Newcastle scholarship held by Ms. F. Wang.

References

1. Rao BK, Jena P (1988) Int J Quantum Chem Symp 22:287
2. Stwalley WC, Koch ME (1980) Opt Eng 19:71
3. Koutecky J, Fantucci P (1986) Chem Rev 86:539
4. Kappes MM, Schlar M, Radi P, Schumacher E (1985) J Chem Phys 84:1863
5. Brechignac C, Cahuzac Ph, Roux JPh (1986) Chem Phys Lett 127:445
6. Gaspar R, Tamassy-Lentei I (1978) Acta Physica Academic Scientiarum Hungaricae 44:191
7. Pavolini D, Spiegelmann F (1987) J Chem Phys 87:2854
8. Searles DJ, von Nagy-Felsobuki EI (1991) J Chem Phys 95:1107
9. Wang F, Searles DJ, von Nagy-Felsobuki EI (1992) J Mol Struct (Theochem) 272:73
10. Wang F, Searles DJ, von Nagy-Felsobuki EI (1992) J Phys Chem 96:6158
11. Wang F, Searles DJ, von Nagy-Felsobuki EI (1992) Mol Phys 77:1197
12. Searles DJ, von Nagy-Felsobuki EI (1991) In: Durig DR (ed) Vibrational spectra and structure, vol 19. Elsevier, Amsterdam
13. Carney GD, Porter RN (1980) Phys Rev Lett 45:537
14. Miller S, Tennyson J, Sutcliffe BT (1989) Mol Phys 66:429
15. Carrington A, Kennedy RM (1984) J Chem Phys 81:91
16. Weis B, Carter S, Rosmus P, Werner HJ, Knowles PJ (1989) J Chem Phys 91:2818
17. Wang F, von Nagy-Felsobuki EI (1992) Aust J Phys 45:651
18. Sutcliffe BT (1990) In: Wilson U (ed) Methods of Computational Chemistry, vol 5. Plenum Press, NY
19. Watson JK (1968) Mol Phys 15:479
20. Watson JK (1970) Mol Phys 19:465
21. Tennyson J, Sutcliffe BT (1984) Mol Phys 51:887
22. Carney GD, Porter RN (1976) J Chem Phys 65:3547
23. Carney GD, Langhoff SR, Curtiss LA (1977) J Chem Phys 66:3724

24. Henderson JR, Miller S, Tennyson J (1988) Spectrochimica Acta A 44:1287
25. Searles DJ, von Nagy-Felsobuki EI (1989) Aust J Chem 42:737
26. Dunne SJ, Searles DJ, von Nagy-Felsobuki EI (1987) Spectrochimica Acta A 43:699
27. Searles DJ, Dunne SJ, von Nagy-Felsobuki EI (1988) Spectrochimica Acta A 44:505
28. Frisch MJ, Head-Gordon M, Schlegel HB, Ragavachari K, Binkley JS, Gonzalez C, DeFrees DJ, Fox DJ, Whiteside RA, Seeger R, Melius CF, Baker J, Martin R, Kahn LR, Stewart JJP, Fluder EM, Topiol S, Pople JA (1988) GAUSSIAN 88, Gaussian Inc, Pittsburgh, PA
29. Langhoff SR, Davidson ER (1974) Int J Quantum Chem 8:61
30. Huzinaga S, Klobukowski MJ (1988) J Mol Struct (Theochem) 167:1
31. Harris DO, Engerholm GG, Gwinn WD (1965) J Chem Phys 43:1515
32. Dunham JL (1932) Phys Rev 41:721
33. Simons G, Parr RG, Finlan JM (1968) J Chem Phys 59:5199
34. Ogilvie JF (1981) Proc R Soc London Ser A 378:287
35. Searles DJ, von Nagy-Felsobuki EI (1991) Phys Rev A 43:3365
36. Searles DJ, von Nagy-Felsobuki EI (1992) Comput Phys Commun 67:527
37. Doherty G, Hamilton MJ, Burton PJ, von Nagy-Felsobuki EI (1986) Aust J Phys 39:749
38. Watson JKG (1977) J Chem Phys 48:181
39. Wolfsberg M, Massa AA, Pyper JW (1970) J Chem Phys 53:3138
40. Kroto HW (1975) Molecular rotation spectra. Wiley, NY
41. The only method to calculate a CI dipole moment in GAUSSIAN 88 is to use the KEYWORD FORCE. However, due to limitations on disk stroage capacity due to the size of the basis set used, this strategy was not feasible. Discrete dipole moment surface available on request from authors
42. John JWC (1987) J Mol Spectrosc 125:442
43. Smith MH, Rinsland CP, Friderich B, Rao KN (1985) In: Rao KN (ed) Molecular spectroscopy: Modern research. Academic Press, Orlando
44. von Nagy-Felsobuki EI, Peel JB (1978) JCS Farad Trans II 74:2204
45. von Nagy-Felsobuki EI, Peel JB (1978) Aust J Chem 31:2571
46. Andriopoulos N, von Nagy-Felsobuki EI (1988) Aust J Phys 41:563
47. Partridge H, Langhoff SR, Bauschlicher CW (1986) J Chem Phys 84:4489
48. Green S (1974) Adv Chem Phys 25:179
49. Penner SS (1959) Quantitative molecular spectroscopy and gas emissivities. Addison-Wesley, Reading